Materials Today Chemistry 24 (2022) 100966

Contents lists available at ScienceDirect

Materials Today Chemistry

journal homepage: www.journals.elsevier.com/materials-today-chemistry/

Pyrrolidine-based catalytic microporous polymers in sustainable C=N and C=C bond formation via iminium and enamine activation

E.L. Vargas [a], N. Esteban [b], J. Cencerrero [a], V. Francés [a], C. Álvarez [c], J.A. Miguel [b], A. Gallardo [c], A.E. Lozano [b, c, d, *], M.B. Cid [a, e, **]

[a] Department of Organic Chemistry, Universidad Autónoma de Madrid, Cantoblanco, 28049 Madrid, Spain
[b] Institute CINQUIMA, Universidad de Valladolid, 47011 Valladolid, Spain
[c] Department of Applied Macromolecular Chemistry, Instituto de Ciencia y Tecnología de Polímeros (ICTP-CSIC), Juan de la Cierva 3, 28006 Madrid, Spain
[d] SMAP, UA-UVA_CSIC, Associated Research Unit to CSIC. Universidad de Valladolid, Facultad de Ciencias, Paseo Belén 7, E-47011 Valladolid, Spain
[e] Institute for Advanced Research in Chemical Sciences (IAdChem), Spain

ARTICLE INFO

Article history:
Received 20 January 2022
Received in revised form
18 April 2022
Accepted 24 April 2022
Available online 15 June 2022

Keywords:
Microporous polymer networks
Pyrrolidine confined catalysts
Iminium catalysis
Enamine catalysis
Green solvents

ABSTRACT

A new set of catalytic materials having a pyrrolidine moiety confined in microporous organic polymer networks (POPs) has been attained. These catalytic polymers have been prepared by a straightforward synthesis starting from microporous polymer networks made from isatin (or a mixture of isatin and trifluoroacetophenone) and 1,3,5-triphenylbenzene. The polymers efficiently catalyzed the formation of nitrones under very mild and sustainable conditions using green solvents through an iminium ion activation mechanism. The reactions are scalable, and polymers are easily recycled. Special attention has been paid to understanding all the factors that could affect the efficiency of the confined catalysts. The electronic and conformational characteristics of the pyrrolidine moiety attached to the porous polymers, as well as other features that could affect the transport through the network, such as molecular volume and shape of reactants and products, and even hydrophilic or hydrophobic properties, have been systematically evaluated. In addition, the heterogeneous polymers are also useful in C=C bond formation through both iminium ion and enamine activation.

1. Introduction

One of the priorities of scientific research today, especially in the chemical and pharmaceutical industries, is the search for technologies that are safer, highly selective, greener, and environmentally friendlier. In this regard, high-performance catalysis, both in a homogeneous and heterogeneous form, plays a fundamental role in meeting these challenges [1–6]. In particular, the use of recyclable catalysts for organic synthesis, with the intention of reducing waste production and optimizing their efficiency, has been widely studied in the last decades [7–11]. Moreover, important advances have been made in heterogeneous catalysts by the confinement of catalysts in microporous cavities, which has given rise to materials that have high TON and TOF properties, excellent selectivity, and high recyclability [12–18]. It has also been confirmed that the confinement of a catalytic center produces an enzyme-like environment, which is translated to a variation in the energetic and kinetic properties of the catalytic process, which should improve the yield and selectivity of the chemical reaction [13,16,19–21].

Enormous progress has been witnessed in the area of homogeneous organocatalysis and particularly in the asymmetric version [22–25], although, to a lesser extent, heterogeneous organocatalysis has also been studied in order to enable the separation and recycling of the catalysts [26].

The simple and sustainable formation of the C=N bond is important due to its application in the fields of chemistry and biology, as well as precursors of the ubiquitous C–N moiety present in nature and many important drugs. Applying the concept of iminium activation followed by transamination reaction [27], we have demonstrated that pyrrolidine is a very effective catalyst in the preparation of all types of C=N bonds, such as imines [28], nitrones [29], as well as oximes or hydrazones [30,31]. The development of a robust and reactive pyrrolidine-based heterocatalyst should provide a very powerful and sustainable tool to form C=N

* Corresponding author.
** Corresponding author.
E-mail addresses: lozano@ictp.csic.es (A.E. Lozano), belen.cid@uam.es (M.B. Cid).

https://doi.org/10.1016/j.mtchem.2022.100966

bonds. However, reaching this goal will require a different design and requirements than those present in traditional proline derivatives that have been created for the purpose of achieving stereoselectivity in enantioselective C–C bond formation processes [26].

Common polymeric (resins) substrates for heterogeneous catalysts do not have well-defined pores. In addition, they have certain disadvantages, such as limited diffusion or swelling of the polymer in the solution used to make the reaction. Due to these drawbacks, among the possible platforms to support pyrrolidine units, we have focused on porous organic polymers (POPs). In general, POPs have excellent efficiency as heterogeneous catalysts due to properties such as high microporosity with high specific surface area and adjustable pore volumes, and also the possibility of incorporating high catalyst loads. Compared to high-ordered and crystalline metal-organic frameworks (MOFs) or covalent organic frameworks (COFs), POPs are amorphous materials, which means that, in theory, their pore sizes have a wider distribution, which could present certain disadvantages, especially for asymmetric catalysis. However, well-designed POPs, constructed from rigid and symmetric monomers, have a well-regulated topological composition that can be tailored, and they could give rise to advanced catalytic materials. An additional advantage is that many POPs have high chemical stability and are easy to prepare [20,31–37]. Regarding the preparation of catalytic POPs, we can distinguish three different strategies: (1) POPs that are derived from monomers having the catalyst attached to their structure, (2) POPs that undergo a process of modification after synthesis to incorporate the catalytic center and (3) POPs that merely encapsulate the catalyst inside their structure.

Several pyrrolidine-based COFs [38–40] and POPs [41] have been described in the context of asymmetric catalysis. In all the cases, the pyrrolidine moiety is anchored through an asymmetric C2 position, close to the reactive center, searching for maximum induction. Regarding our research, as no stereogenic centers are created in the formation of C=N, the pyrrolidine moiety could be anchored through the C3 position to the well-tailored POPs. This type of linkage should improve the accessibility to the reactive center and therefore increase the catalytic activity [26]. For the preparation of the C3-linked pyrrolidine POPs, we decided to use the more versatile option 2 mentioned above. This strategy implies the synthesis of a scaffold where we can incorporate different catalytic moieties. In addition, this methodology allows us to study the effect of the *nanohole* without a catalytic center, before the functionalization process, in order to evaluate the role of confinement in the catalytic processes. Nevertheless, we are conscious that this is a very difficult parameter to be evaluated independently as other factors also compete with a confinement effect in the catalytic process. For facilitating this assessment, simple non-polymeric models have also been prepared and the confinement effect was analyzed in some cases.

Regarding the relevance of C=N bond formation, we especially consider the interesting formation of nitrones as they are valuable intermediates in organic synthesis [42], and also the free radical trapping agents that reduce damage in some biological systems [43,44], and are thus very attractive potential therapeutic agents [45].

We present herein the development of new pyrrolidine-based heterogeneous POPs, which have exhibited a high efficiency and recyclability using green solvents in the formation of nitrones in a preparative way. Although the new polymer networks were prepared to be effective in C=N bond formation, we have also shown that they are useful in C=C bond-forming reactions such as Knoevenagel or aldol reactions followed by dehydration. This high efficiency in catalyzing the formation of C=N and C=C from carbonyl compounds via both iminium and enamine activation is plausible due to an appropriate balance of catalyst loading and pore size of the free volume elements. Additionally, we have performed a thorough and systematic study mainly based on experimental observation and theoretical calculations to analyze all the factors affecting catalysis. Rationalizing all these aspects, as well as others like hydrophobic/lipophilic balance and transport facility, would help to understand the effect of confinement and will help to progress in the design of other enzyme-like efficient and sustainable polymeric catalysts. The properties of these rigid pyrrolidine-confined polymers should permit their use in flow-synthesis employing high pressures.

2. Results and discussion

2.1. Synthesis of heterogeneous confined catalysts

The precursor porous polymer network (IB, I=Isatin, B = 1,3,5-triphenylbenzene) was made by reaction of 1,3,5-triphenylbenzene (1,3,5-TPB) and isatin using a stoichiometric ratio of functional groups (2/3) and triflic acid as reaction promoter, as depicted in Scheme 1. The polycondensation reaction proceeded with quantitative yield and is related to the Zolotukhin-Klumpp methodology [46–48] by reaction of ketones, having electron-withdrawing groups (i.e.; isatin, trifluoroacetophenone, etc.), with rigid and symmetric polyfunctional aromatic monomers (i.e.; triptycene, 1,3,5-triphenylbenzene, tetraphenyl methane, etc.) employing very low pK_a acids, as the promoter media [49].

In the first stage, (*R*)-(−)-*N*-Boc-3-pyrrolidinol and *N*-Boc-3-hydroxymethylpyrrolidine were easily converted to the mesylate derivatives (see Supporting Information) to provide the compounds P_0 and P_1, having or not a methylene spacer, respectively. These pyrrolidine derivatives were anchored to the lactam of the porous polymer through a straightforward and regioselective bimolecular nucleophilic substitution to provide **IBP$_0$-Boc** and **IBP$_1$-Boc,** respectively. Finally, TFA was used to deprotect the *tert*-butoxycarbonyl (Boc) group, and the corresponding trifluoroacetate salt was liberated by washing the polymer with a pH $\geq$ 10 carbonate solution, affording the heterogeneous catalysts **IBP$_0$** and **IBP$_1$**, which differ in the presence or not of a methylene group as the link between the pyrrolidine catalyst moiety and the POP support.

Moreover, in order to reduce the number of catalytic sites per repeat unit, a microporous copolymer made by mixing an equimolecular amount of isatin and trifluoroacetophenone was prepared by reaction with 1,3,5-TPB using the same methodology as for **IBP$_0$** and **IBP$_1$** to form the catalytic copolymers, **IBTP$_0$** and **IBTP$_1$.** Finally, a porous polymer network, **IBMe**, derived from **IB**, in which the H of the lactam group was replaced by a methyl group, was obtained to determine the importance of hydrogen of the lactam moiety in the catalytic process.

For the sake of clarity, Fig. 1 gathers all the polymers that have been used for the catalysis via iminium and enamine activation. The prepared polymers **IBP$_0$**, **IBP$_1$**, **IBTP$_0$**, **IBTP$_1$**, were named according to their initials: **I** = isatin, **B** = 1,3,5-triphenyl**b**enzene, **P** = pyrrolidine and **T** = trifluoroacetophenone (TFAP). The suffix $_1$ has been added when the structure has a methylene bridge link between the porous polymer lactam and the pyrrolidine moiety in its structure. Therefore, **IB** and **IBT** correspond to the precursor skeletons of the corresponding series of heterogeneous catalysts. Moreover, the heterogeneous polymer **IBMe**, having an *N*-methyyl lactam moiety, was tested to figure out the effect of confinement, eliminating the possibility of any hydrogen bond catalysis. Finally, in order to assess the catalytic activity of the structural unit without the confinement effect, several homogeneous model catalysts (**IM**)

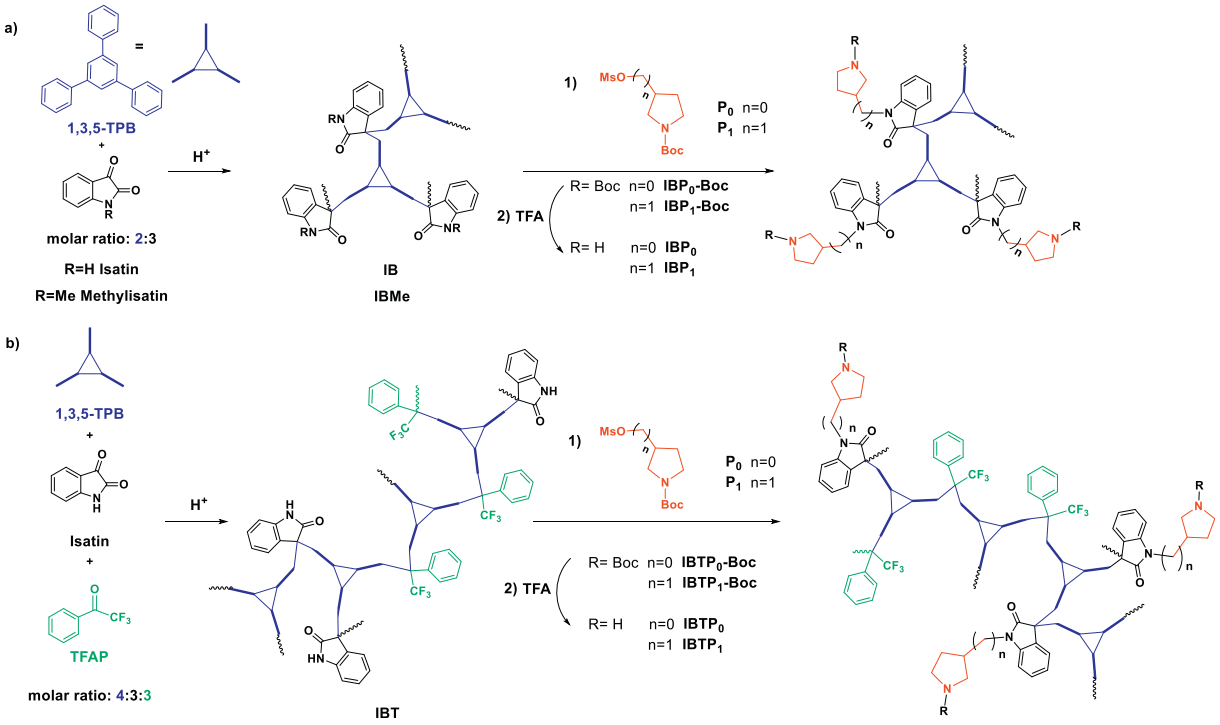

Scheme 1. Preparation of pyrrolidine functionalized porous polymers and precursors.

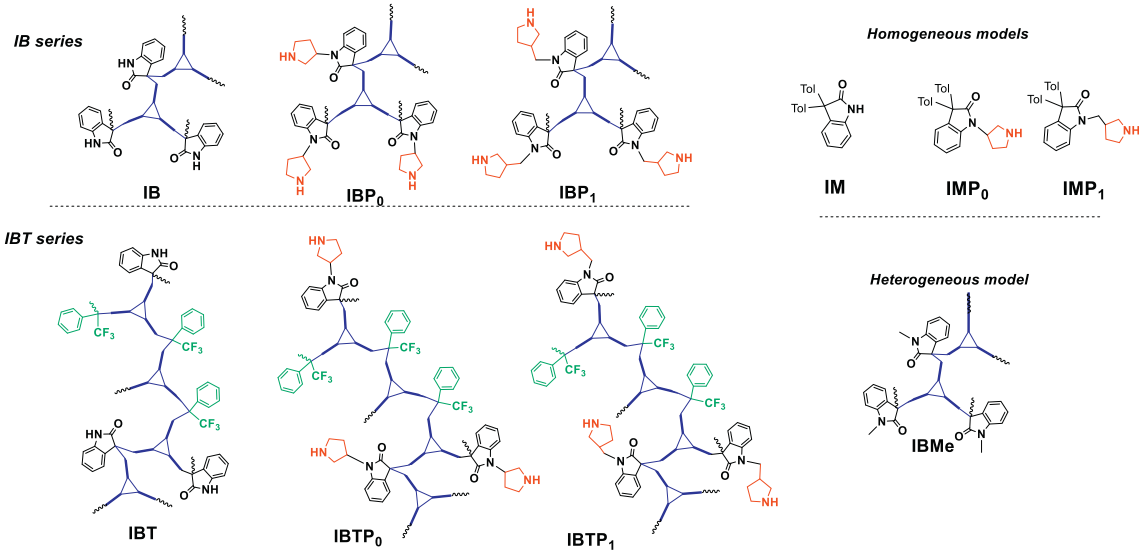

Fig. 1. List of tested heterogeneous and homogeneous catalysts.

were prepared. The condensation of isatin (**I**) and toluene provided the precursor **IM** that, by the incorporation of the pyrrolidine moieties, provided compounds **IMP$_0$** and **IMP$_1$,** respectively.

2.1.1. Polymer characterization

The precursor polymers, **IB** and **IBT**, which were obtained with almost quantitative yield, showed excellent thermal and chemical stability. Additional details and characterization of the polymer precursors have been described elsewhere and are also described in the supporting information section [49].

The TGAs of the catalytic microporous polymer networks **IBP$_0$, IBP$_1$, IBTP$_0$,** and **IBTP$_1$** are depicted in Fig. 2. It can be seen that their thermal stability is high, starting the degradation of the supported pyrrolidine group above 300 °C.

Also, the confined catalysts were extensively characterized in order to confirm their functionalization, as it is discussed here. In this regard, dynamic TGA has proven to be a very useful tool to confirm pyrrolidine functionalization, as well as to quantify it. As **IBP$_0$, IBP$_1$, IBTP$_0$,** and **IBTP$_1$** are thermally stable polymers, the Boc groups can be thermally removed [50,51]. Thermal elimination of Boc is observed in **IBP$_0$-Boc**, **IBP$_1$-Boc, IBTP$_0$-Boc,** and **IBTP$_1$-Boc** polymers, as a differential weight loss centered at 200–250 °C (Figs. S44, S50, S63, and S64, supporting information section), confirming the presence of t-BOC protected pyrrolidine groups, and

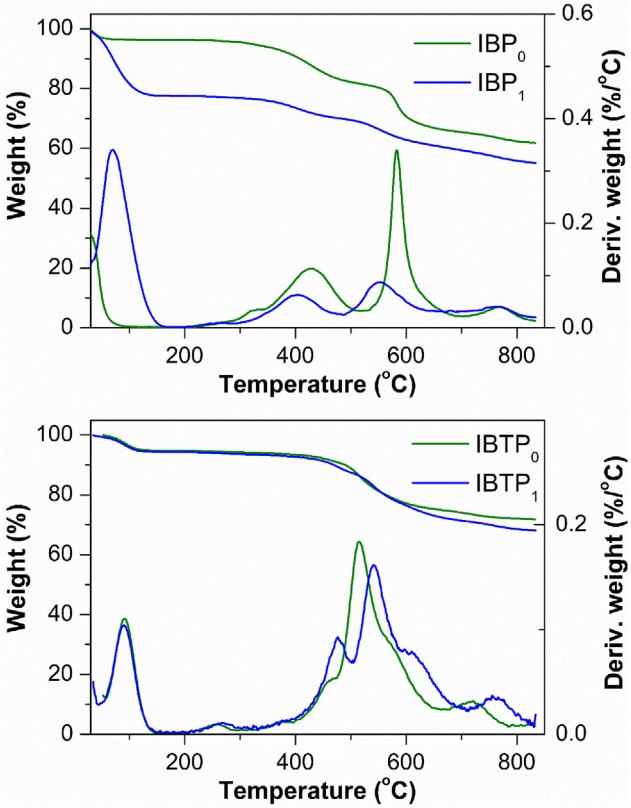

Fig. 2. Dynamic thermograms of IB catalyst polymers, IBP_0 and IBP_1 (top graph), and IBT catalyst polymers, $IBTP_0$ and $IBTP_1$ (bottom graph).

therefore, confirming the functionalization of the precursor POPs. The deprotected polymers no longer show this differential peak (Fig. 2). Furthermore, the relative weight loss can be used to calculate the degree of functionalization and its actual catalytic loading. The functionalization results (catalytic loads) were those seen in Table 1. A detailed description of the method employed for determining the catalytic load is thoroughly described in the supporting information section.

Analysis of CPMAS SS ^{13}C NMR and IR spectra of **IBP_0** and **IBP_1** (Figs. 3 and 4) have confirmed the functionalization. CPMAS SS ^{13}C NMR spectra show an aliphatic region that has to be assigned to pyrrolidine (or in the case of **IBP_1**, both to the pyrrolidine group and the methylenic spacer). In the case of **IBP_0**, inside this region, a peak centered at 30 ppm may be assigned to the ring CH_2 not linked to N ($CH-\boldsymbol{CH_2}-CH_2$), while the group of peaks centered at around 50 ppm can be assigned to the ring CH_2 linked to N. Peak at 63 ppm may be assigned to aliphatic $-CH <$ groups. Besides the aromatic region that exhibits three wide peaks in the region 105–150 ppm, the peak at 179 ppm can be assigned to the lactam carbonyl group. In the case of **IBP_1**, the CPMAS SS ^{13}C NMR spectrum is similar to the spectrum of **IBP_0**, although some differences may be pointed out. In the aliphatic region, the peak observed at the lower field (in this case centered at 45 ppm) is more intense than in the case of **IBP_0** (as compared to the peak centered at 30 ppm), which agrees with the inclusion of spacer $N-CH_2$-Py to that peak centered at 45 ppm. The peak centered at 80 ppm has been associated with $CDCl_3$. In this case, the lactam C=O peak is less intense. It has to be noted that these spectra agree with the ^{13}C NMR spectra of the related models **IMP_0** and **IMP_1** (Figs. S38 and S41), which show the different aliphatic, aromatic, and C=O peaks indicated above. IR spectra also exhibit aliphatic peaks between 2750 and 3000 cm^{-1}, which can be assigned to the pyrrolidine ring and the methylene spacer. Again, these results agreed with the IR spectra of the models **IMP_0** and **IMP_1** (Figs. S39 and S42). IR spectra also show, in addition to the fingerprint region below 1500 cm^{-1}, peaks assigned to the lactam group (1650–1750 cm^{-1}) (see Figs. 3 and 4).

Table 1
Degree of functionalization of the four catalytic-supported polymer networks.

Polymer network	IBP_0	IBP_1	$IBTP_0$	$IBTP_1$
Pyrrolidine Functionalization degree (Pym%)	64.2	68.5	48.4	67.3
Catalytic load (mmolPy/g POP)	1.79	1.75	0.67	0.90

Analysis of the CPMAS SS ^{13}C NMR and IR spectra of **$IBTP_0$** and **$IBTP_1$** (Figs. S55, S56, S59, and S60, supporting information section) agrees with the above discussion both in determining the structural features and in calculating the functionalization ratio. Since these are copolymers, and there is less intrinsic pyrrolidine charge, the aliphatic region signals in the CPMAS SS ^{13}C NMR spectra appear less intense.

The porosity of **POPs** was determined by measuring N_2 adsorption conducted at the boiling temperature of nitrogen (77 K) (Fig. 5). Thus, **IB** and **IBT** POP precursors showed a specific Brunauer-Emmet-Teller (BET) surface area of 794 m^2/g and 738 m^2/g, respectively.

The **IBPn** and **IBTPn** catalysts showed a high specific surface area, with **IBPn** values being lower than those of **IBTPn**, but in any case, all of them showed BET specific surface areas higher than 500 m^2/g. In addition, they were microporous materials with average pore sizes near 2 nm. Details of the porous properties are included in the characterization section of this manuscript.

In addition, details of the pK_a calculations are included in the Electronic Supporting Information section.

2.2. Study of the catalytic activity

2.2.1. C=N bond formation via iminium activation. Synthesis of nitrones

One of the most employed methods to prepare nitrones is based on the condensation of aldehydes and the corresponding nitrogenated derivatives. Because of the low stability of the free *N*-monosubstituted hydroxylamines, the condensation strategies generally start from the liberation of the corresponding hydrochloride salts by treatment with base. The method described by us employs pyrrolidine both as base and catalysts, allowing the use of stoichiometric amounts of reagents (aldehyde and hydroxylamine) under very mild and simple conditions, avoiding purification steps [29]. However, the use of the heterogeneous catalyst that would allow a more environmentally friendly approach requires reoptimization and the use of an additional base to liberate the hydrochloride salt. Therefore, we evaluated the performance of the **IBP_0** polymer using different solvents and bases and *p*-chlorobenzaldehyde 1a and *N-tert*-butylhydroxylamine hydrochloride **2a** as model substrates. Table 2 gathers some results obtained in the optimization process, which is thoroughly discussed in Table S4 of the Supporting Information section.

The polymer not only efficiently catalyzed the formation of nitrones in organic solvents (entry 1) but also in a green mixture of solvents (water/alcohol) (entries 2,3,5). $NaHCO_3$ turned into the most efficient base when using the **IBP_0** polymer providing high yields (entry 2) even employing a low catalyst loading (entry 3). The role of $NaHCO_3$ as a simple base and no as a catalyst was demonstrated in entry 4. When EtOH was used instead of MeOH, the reaction was faster and efficient (entry 5).

We proved that under conditions of entry 5 the reaction is scalable to more than 1 g of aldehyde using polymer **IBP_0** (0.07 equiv) to

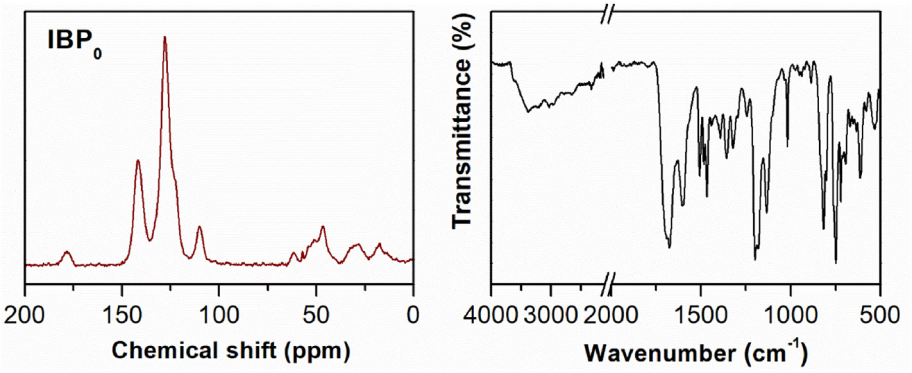

Fig. 3. (left graph) CPMAS SS ^{13}C NMR of **IBP_0**. (right graph) FTIR-ATR of **IBP_0**.

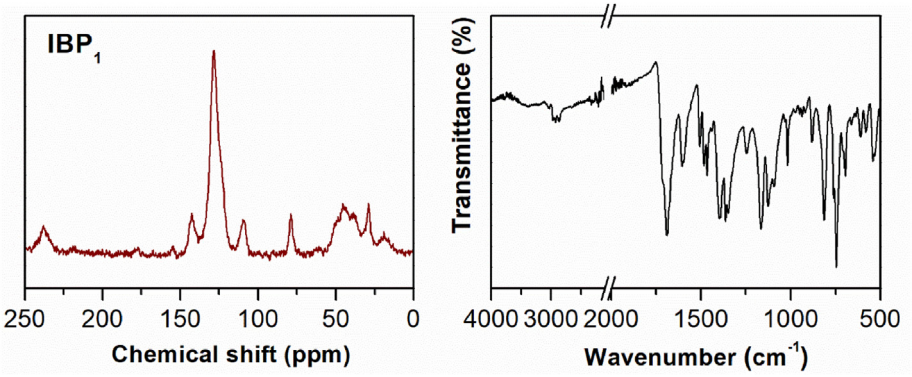

Fig. 4. (left graph) CPMAS SS ^{13}C NMR of **IBP_1** (right graph) FTIR-ATR of **IBP_1**.

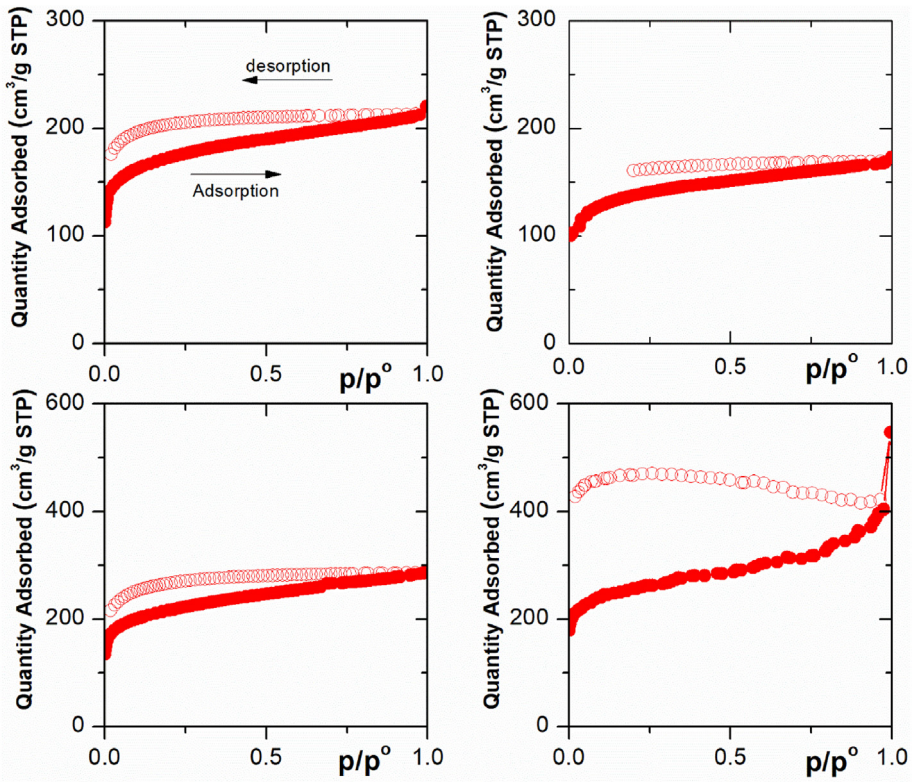

Fig. 5. Adsorption/desorption isotherms plots of; **IBP_0** (top left), **IBP_1** (top right), **$IBTP_0$** (bottom left) and **$IBTP_1$** (bottom right).

Table 2
Reaction of *p*-chlorobenzaldehyde and *N*-*tert*-butylhydroxylamine hydrochloride.

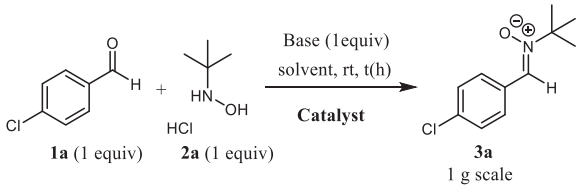

Entry	Base (1 equiv)	Cat (equiv)[a]	Solvent	Time (h)	Conv. % (yield %)
1	Et_3N	**IBP_0** (0.15)	DCM	4.5	98 (**87**)[d]
2	$NaHCO_3$	**IBP_0** (0.15)	H_2O/MeOH[b]	18	100 (**79**)[d]
3	$NaHCO_3$	**IBP_0** (0.07)	H_2O/MeOH[b]	18	98
4	$NaHCO_3$	–	H_2O/MeOH[b]	18	0
5	$NaHCO_3$	**IBP_0** (0.07)	H_2O/EtOH[c]	5	98 (**89**)[d,e]

Reaction conditions: 1a (0.2 mmol), 2a (0.2 mmol), base (0.2 mmol), solvent (0.6 mL) at 25 °C.
[a] Considering the real pyrrolidine load according to the calculated effective molecular weight (*MW*_eff) of the polymer.
[b] A mixture of H_2O/MeOH (1:1).
[c] A mixture of H_2O/EtOH (1:1).
[d] Yield after column chromatography.
[e] Reaction performed in 1 g scale afforded the same yield.

provide nitrone **3a** after 7 h, a slightly longer reaction time than when the reaction was performed in a lower scale (5 h). The polymer was recovered by filtration, washing using ULTRA-TURRAX, followed by filtration under vacuum. The comparison of the CPMAS SS ^{13}C NMR and FTIR of the recovered and pristine **IBP_0** showed very small changes demonstrating the integrity of the structure of the polymer and the pyrrolidine moiety after catalysis (Figs. S8 and S9). The comparison of BET also indicates that the porous features have not been modified substantially (see Supporting information).

Once demonstrated the scalability of the **IBP_0** polymer, the catalytic activity of the rest of the polymers was tested (Table 3). We evaluated the role of the substituents surrounding the pyrrolidine moiety and the effect of the confinement. For that purpose, we analyzed the mentioned polymers with different types of unions to pyrrolidine and load of the pyrrolidine catalyst: **IBP_1**, **$IBTP_0$**, **$IBTP_1$** (entries 2–4), the precursor skeleton with no pyrrolidine **IB** and **IBT**, as well as the corresponding *N*-methyl lactam network polymer **IBMe**, which is not able, as commented above, to perform any hydrogen bond catalysis (entries 5–7).

Moreover, all the corresponding homogeneous models **IM**, **IMP_0**, and **IMP_1** were also studied (entries 8–10). It is important to note that all the reactions were stopped at 30 min to avoid total conversions and thus to be able to unequivocally evaluate the performance of the different polymers.

The **IBP_1** polymer having the methylene bridge between the pyrrolidine unit and the lactam moiety of the porous polymer provides higher conversions than the **IBP_0** polymer (compare entries 1 and 2). The **IBT** series, which has a lower pyrrolidine concentration, provided lower conversions than their **IB** counterparts (compare **IBP_0** with **$IBTP_0$** in entries 1 and 3), as well as **IBP_1** with **$IBTP_1$** (entries 2 and 4). Interestingly, the polymers that do not contain pyrrolidine units, **IB** and **IBT,** showed some conversion to nitrone **3a** (entries 5 and 6). This catalytic effect is difficult to explain, but it could be due to the existence of a confining effect of the porous structure of the polymer and/or to the existence of hydrogen bond catalysis exerted by the NH of the lactam moiety. The lower conversion observed with **IBMe** (entry 7), which lacks the possibility of an H-bond, suggests the existence of an H-bond catalysis effect. The slightly higher conversion showed by **IBMe** (entry 7) compared with the control experiment in the absence of

Table 3
Reactions of *p*-chlorobenzaldehyde and *N*-*tert*-butylhydroxylamine hydrochloride.

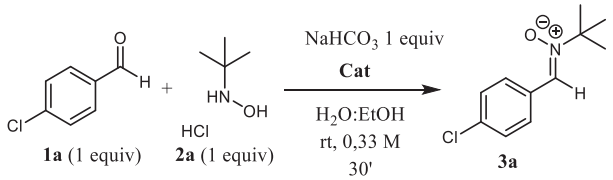

Entry	Catalyst		Conversion (%)H_2O/EtOH	EtOH[d]
1	Pyrrolidine-Based	IBP_0[a]	52	65
2	Porous Polymers	IBP_1[a]	73	60
3		$IBTP_0$[b]	29	
4		$IBTP_1$[a]	58	
5	Porous-Polymers	IB[c]	38	
6	without pyrrolidine	IBT[c]	31	
7		IBMe[c]	21	
8	Homogeneous models[d]	IMP_0[c]		78
9		IMP_1[c]		72
10		IM[c]		38
11		–	12	11
12	Controls	pyrrolidine[c]	86	

Reaction conditions: **1a** (0.2 mmol), **2a** (0.2 mmol), base (0.2 mmol), H_2O/EtOH (1:1) (0.6 mL) at 25 °C for 30 min. For more detailed conditions, see SI. Considering the real pyrrolidine load according to the calculated effective molecular weight (*MW*_eff) of the polymer.
[a] 7 mol %.
[b] 5 mol %.
[c] 10 mol % and.
[d] homogeneous catalysts were not soluble in the H_2O/EtOH solvent mixture.

catalysts (entry 11) also could suggest some confinement effect. The homogeneous models did not have enough solubility in the EtOH/H_2O mixture, and therefore homogeneous, and the best heterogeneous catalysts had to be tested in pure ethanol (right column). As can be seen in entries 8 and 9, the homogeneous models provided slightly higher conversions (30 min reactions) than the polymers **IBP_0** and **IBP_1**, which afforded similar results among them (entries 1 and 2, right column), but slightly different according to the solvent (left and right columns). Therefore, although the result obtained using pyrrolidine (entry 12) is superior, polymers **IBP_0**, **IBP_1,** and **$IBTP_1$** (entries 1, 2, and 4) are a useful and sustainable alternative. In fact, we demonstrated that polymer **IBP_1** was reusable for at least 7 cycles without any decrease in efficiency (yields around 80–90%). We started from 50 mg of polymer, equivalent to 0.09 mmol of catalytic pyrrolidine polymer, and after 5 h of reaction, to ensure complete consumption of the starting material, the polymer was recovered. It is important to note that after each cycle, the recovery of the polymer material by filtration involves an inevitable loss of mass. The weight of employed reagents was recalculated to the amount of recovered polymer (for a more detailed information, see Table S5 of supporting information). As no significant drop in the reaction yield is observed, we believe that the catalyst is very stable and that these results could be extended to reactions operating under flow conditions.

Once the value of the new sustainable heterogeneous catalysts was established, we decided to systematically analyze all the factors that could affect their efficiency. These studies include the evaluation of the electronic and conformational differences of the pyrrolidine moiety attached to the porous polymers in comparison with unsubstituted pyrrolidine. We also assessed other features that could affect the transport through the free volume elements of the networks, such as molecular volume and shape and even hydrophilic or hydrophobic properties of polymer networks, reagents, and products.

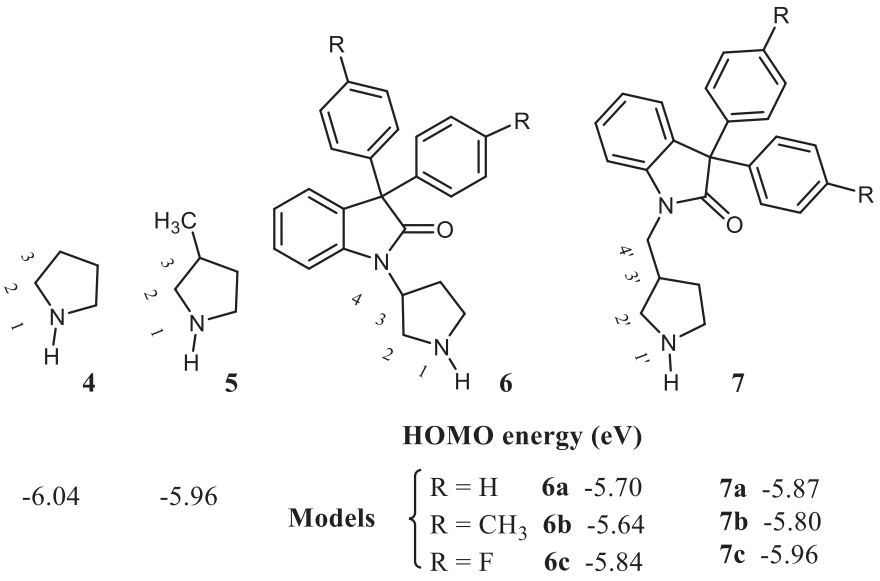

Fig. 6. HOMO energy values (eV) of modeled structures.

2.2.2. Theoretical calculations

In order to understand the effect of the isatin aromatic framework on the features of the pyrrolidine moiety, we performed some theoretical calculations paying attention to nucleophilicity, geometry, and electrophilicity/stability of the iminium ion intermediate. In the first stage, the electronic and energetic parameters of pyrrolidine (**4**), as well as of the pyrrolidine models represented in Fig. 6 were determined. Specifically, all of these models are 3-substituted pyrrolidine (**5**) moieties, and they were similar to the polymeric structures without (**6a-c**) and with methylene group (**7a-c**). In addition, modifications of the original models (R = H) were also performed by changing the substitution of the 4-position at the aromatic rings (R = CH_3, F) in order to quantify the electronic effects on the pyrrolidine moiety. It was observed that models with and without the link CH_2 group (**6**) showed the highest HOMO energy values, and therefore they should be more nucleophilic than the rest of the studied derivatives (HOMO = −5.64−5.84 eV).

From the conformational point of view, some interesting features were observed. In the model without the methylene linker CH_2 (n = 0), the isatin framework moiety sets the conformation of the pyrrolidine group (**6a**), forming a dihedral angle α (1,2,3,4, Fig. 7a) of −36.19°, while that for the one with the CH_2 group, the angle α value (1',2',3',4', Fig. 7b) was −46.88° (**7a**). Thus, it seems that the attached pyrrolidine groups with CH_2 spacer possess a more marked envelope shape, which, in turn, increases the availability of the electron pair in the nucleophilic nitrogen. Another interesting conformational data is that the model that does not have the CH_2 link (**6a**) presents a stabilizing interaction between the nitrogen of the pyrrolidine moiety and the carbon of the lactam group, which could decrease its nucleophilicity.

In addition, the electronic and Gibbs energies of electrophiles (aldehydes and iminiums) were calculated. For the sake of simplicity (to shorten the computational cost), a series of models of iminium derivatives were modeled to determine how the C=N bond varies with different substituents. The LUMO energy values are collected in Table 4 and will be commented on below. Furthermore, a simplified reactivity pathway of nitrone formation was performed using a reactivity probe as shown in the Supporting Information section.

2.2.3. Stereoelectronic and hydrophobic effects

The effect of the molecular volume and shape of the aldehydes, as well as the nature of the substituents in the catalytic process, was evaluated by varying the substituent at the *para* position of benzaldehyde using the polymers **IBP_0** and **IBP_1**. Regarding the effect of every substituent in the conversions, several aspects should be considered in order to rationalize the observed results. Thus, understanding all the parameters that determine the behavior of these polymeric materials is fundamental to improving their properties in future designs. Therefore, we also represent in Table 4

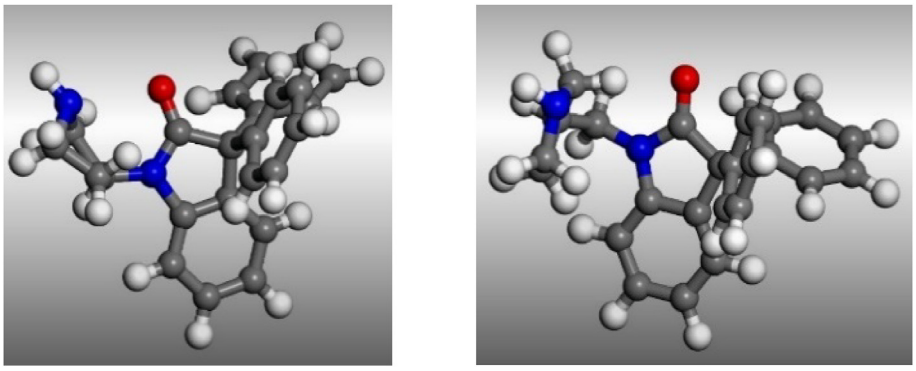

Fig. 7. (left graph) Molecular depiction of model **6a**. (right graph) Molecular depiction of model **7a**.

Table 4
Formation of nitrones of different aromatic aldehydes using **IPB_0** and **IPB_1** as catalysts.

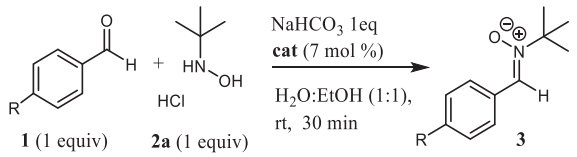

Entry	R	1 E_{LUMO}[b]	Iminium[c] E_{LUMO}[b]	HLB 1	HLB 3	Conv.[a] IBP_0[d]	IBP_1[d]
1	**Cl (a)**	−2,00	−6,51	4.14	2.84	52	73
2	**H (b)**	−1,73	−6,42	5.48	3.39	65	93
3	**F (c)**	−1,77	−6,43	4.68	3.08	47	100
4	**CH_3(d)**	−1,61	−6,22	4.84	3.14	61	85
5	**CF_3(e)**	−2,24	−6,73	3.34	2.45	43	100
6	***t*Bu (f)**	−1,59	−6,12	3.58	2.58	24	32
7	**MeO(g)**	−1,40	−5,93	8.88	5.89	37	48
8	**NO_2(h)**	−3,12	−7,09	9.93	6.85	14	22
9	**1-naph (i)**	−2,10	−6,25	3.72	2.64	11	32
10	**2-naph (j)**	−1,89	−6,12	3.72	2.64	19	23

Reaction conditions: **1a** (0.2 mmol), **2a** (0.2 mmol), base (0.2 mmol), catalyst (0.014 mmol), H_2O/EtOH (1:1) (0.6 mL) at 25 °C for 30 min.
[a] Conversion after 24 h.
[b] (DFT B3LYP/6-31G(d,p), (eV).
[c] Iminium ion of pyrrolidine and.
[d] Mol % calculated considering the real pyrrolidine load according to the effective molecular weight (*MW*_eff) of the polymer.

several parameters that were systematically analyzed. The LUMO energies of the aldehydes and pyrrolidine iminium calculated to evaluate electrophilicities are collected in columns 3 and 4. The hydrophilicity/lipophilicity balance of aldehydes **1** and **3** was also calculated [52] and shown in columns 5 and 6. The size/shape of all the starting materials and products is shown in the Supporting Information section. As in the previous case, in order to clearly analyze the trends before the reactions ended, the reactions were stopped after 30 min. Control reactions in the absence of any catalyst were accomplished for all the substrates and commented in Supporting Information section. A general trend observed for all the aldehydes is the higher conversions rendered with the **IBP_1** catalyst than with **IBP_0** one (columns 7 and 8).

As shown in Table 4, experimental conversions of the pyrrolidine catalysts **IBP_0** and **IBP_1** did not follow the same pattern as the expected electrophilicity according to the theoretical energy value of the LUMO orbitals of the corresponding iminium ions. This observation is especially remarkable in the case of the nitro group (**1h**), which presents very low conversions (entry 8). Interestingly, **1h** has a hydrophilic/lipophilic value close to 10, which is around double the value of other aldehydes like **1a-e,** which present much higher conversions. For the naphthyl derivatives, the existence of steric hindrance due to their higher molecular volume should be considered. Furthermore, the experimental differences in the reactivity between the 2-naphthyl (**1j**) and 1-naphthyl (**1i**) substituents could be due to the different shapes of the corresponding nitrones (2-naphthol **3j**, being more linear) and the pore structure of each network polymer (Table S10 included in the Supporting Information section). According to this result, it is expected that ortho-substituted compounds should afford lower conversions. To confirm this hypothesis, we performed the reaction of formation of nitrones using *o*-, *m*- and *p*-toluenebenzaldehyde assisted by the **IBP_0** polymer. As we anticipated, using the same conditions of Table 4, conversions were 35, 63, and 61%, respectively. Thus, it is clear that the behavior of the aldehyde having a methyl group in the ortho position has a reactive behavior similar to that observed with **1i** (1-naphthyl aldehyde), which supports a high steric effect.

According to Table 4, the difference in the HLB (hydrophobic/lipophilic balance) [52] of substrates seems an important issue to be considered. This can be clearly seen in Fig. 8 which represents the HLB of both substrates and products with respect to polymeric catalysts **IBP_0** (in black) and **IBP_1** (in red).

One of the conditions for efficient catalysis in heterogeneous microporous systems is that the products flow easily out of the internal pores of the catalytic material to the outside, but the formation of very bulky molecules could hinder this process, leading to clogging of the material. In addition, the transport of molecules from the surface to the pores is the function of the hydrophilicity/lipophilicity affinity features of the porous material, which could cause some products to leave before others. This fact could determine that the hydrophilic aldehydes having even strong EWG groups like NO_2, provided the lowest conversions (**1g** and **1h**).

It is important to point out that conversions in Table 4 refer to reactions stopped at short reaction times, which was done for mechanistic reasons. Nevertheless, the heterogeneous catalysts were able to promote the reaction until completion, even in the case of those aldehydes that provided low conversions at short reaction times. Following this methodology, we proved that the nitro derivative **1h** afforded complete conversion to the

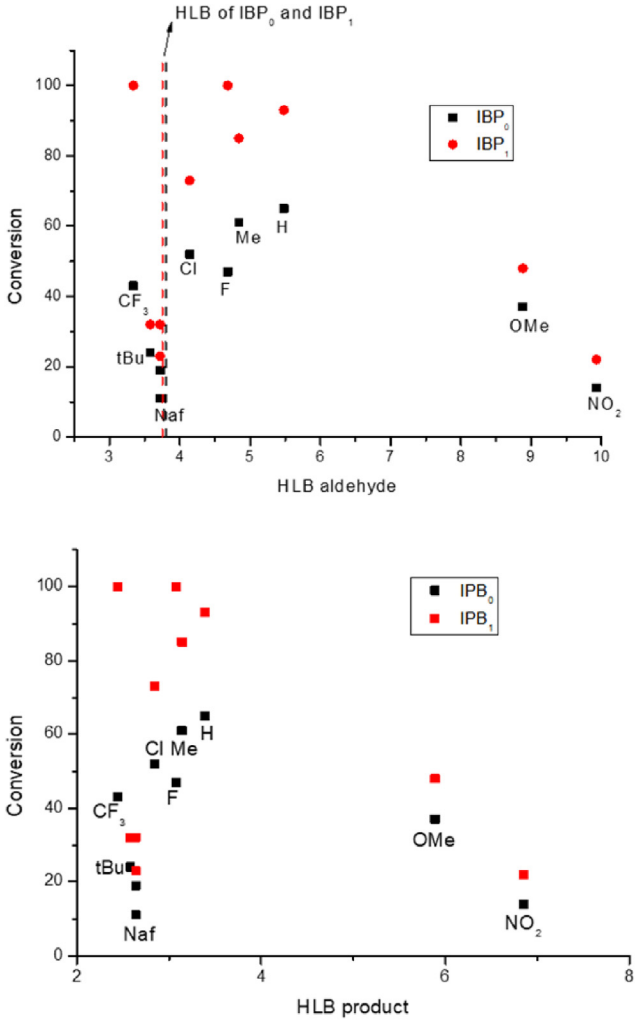

Fig. 8. (top graph) HLB (hydrophobic/lipophilic balance) of substrates. (Bottom graph) HLB of products. Dashed lines correspond to the HLB of polymers.

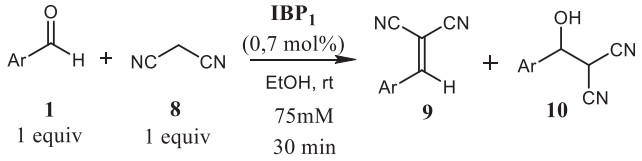

Scheme 2. Study of reactivity of malononitrile with different aromatic aldehydes employing **IBP$_1$**.

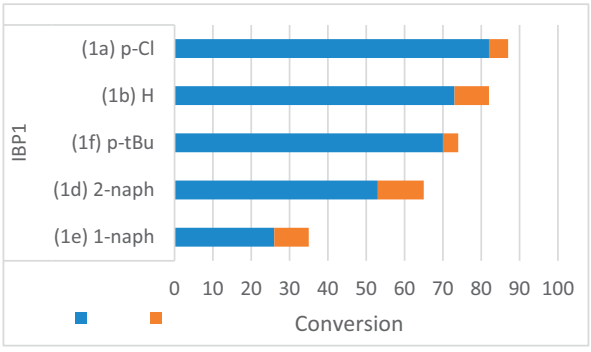

Reaction conditions: **1** (0.9 mmol), **8** (0.9 mmol), catalyst (0.0065 mmol), EtOH (12 mL) at 25 °C for 30 min. The mmol of the catalysts have been calculated considering the real pyrrolidine load according to the effective molecular weight (*MW*_eff) of the polymer.

corresponding nitrone **3h** after 24 h reaction. Nevertheless, aldehyde **1i** only gave a 47% conversion after 24 h, which could indicate that the size/shape of reagents and products is the most determining fact in reaching (or leaving) the catalytic center.

2.2.4. C=C bond formation via iminium and enamine activation

Knoevenagel reaction is a useful reaction frequently chosen in the literature as a standard and feasible model to figure out the activity of heterogeneous catalysts [53]. Therefore, in order to compare the catalytic activity of our **IBP** polymers with some others described in the literature, we also studied the Knoevenagel reaction. We proved that **IBP$_1$** and **IBP$_0$** catalyze the Knoevenagel reaction of aldehydes having different electronic properties, molecular shapes, and molecular sizes with malononitrile (**8**) to provide compounds **9** and/or **10**. Scheme 2 shows the conversions observed when 1mol % of **IBP$_1$** was used with various aldehydes, and the reactions were stopped after 30 min. Slightly longer times provided a synthetically useful method. Although our study provided insight into the intrinsic reactivity of each aldehyde, the background reaction, which was evaluated sin all cases, complicated the interpretation of some parameters that could affect the catalysis and the comparison with other described polymers. All this information is gathered in the Supporting Information section.

Finally, we proved that **IBP** polymers are also useful in enamine catalysis in the aldol condensation. The most representative results are collected in Table 5, which show the behavior of several aldehydes using the **IBP$_0$** polymer as a catalyst, which presented more facility to provide the dehydrated product.

Interestingly, the catalytic performance mainly depends on the electronic properties and on the shape/size/hydrophilicity of aldehydes and products rather than on the LUMO energies. For example, aldehyde **1f** with the lowest electrophilicity provides higher conversion than aldehyde **1b** after 24 h, and the corresponding enone **13** isolated in very high yield (88%). It was also observed that the nature of the aldehyde also affects the aldol **12**/enone **13** ratios. Thus, in the reactions with the bulky aldehydes **1f** and **1i** the

Table 5
Reaction of acetone with different aromatic aldehydes.

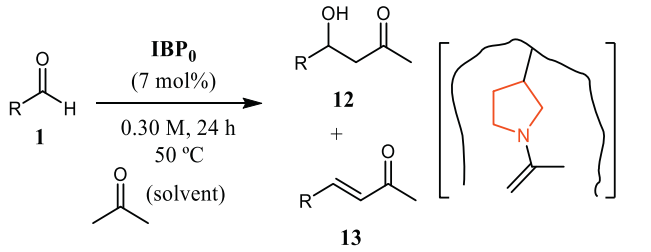

	p-Cl-phenyl 1a	Phenyl 1b	*p*-tBu-phenyl 1f	1-Naphthyl 1i	2-Naphthyl 1j
Conv[a]	100	74	100	11	83
Ratio (12:13)	13:87	75:25	0:100	0:100	56/44
Yield[b]	21/68	51/21	0/88	[c]	49/34
E_{LUMO}[d]	−2,00	−1,73	−1.60	−1.89	−2.01

Reaction conditions: **1** (0.3 mmol), solvent (acetone; 1 mL), 50 °C for 24 h. The mol % of the catalysts has been calculated considering the real pyrrolidine load according to the effective molecular weight (*MW*_eff) of the polymer (1133.3 g/mol).
[a] Conversions measured by ^{1}H NMR.
[b] Yield after column chromatography, and.
[c] Not determined.
[d)] (eV).

corresponding aldols **12** were not detected, which points out a higher tendency to dehydration in the bulkier compounds that increase the HLB (hydrophobic/lipophilic balance) favoring diffusion.

3. Conclusion

A series of well-tailored pyrrolidine-based porous polymers have been easily attained in a straightforward synthetic procedure, which has proven to be very efficient in the formation of C=N and C=C bonds, using both iminium and enamine activation. In the context of the synthesis of nitrones, we have developed an efficient, and extremely simple sustainable method, metal and acid-free, scalable and recyclable. The prepared polymers were also efficient in Knoevenagel reaction and aldol condensation to generate alkenes in a simple way using green solvents. The effect of confinement and the role of non-covalent catalysis through hydrogen bonding activation in each reaction were analyzed by testing a wide battery of heterogeneous catalysts, opening access to the study of other processes. The theoretical study pointed out the importance of the flexibility of the pyrrolidine moiety in the microporous structure due to the existence or not of the methylene bridge, which seems to determine the non-innocent role of the isatin moiety in iminium stabilization.

A set of experiments using different aldehydes allowed us to determine that the size/shape and hydrophobic/hydrophilic balance of the reagents are more determinant factors than those derived from electronic effects in the catalytic process.

The results reported in this work represent a clear novelty for the type of porous materials employed (POP), as well as for the catalytic process; C=N bond formation using iminium activation. This systematic experimental and theoretical analysis has provided us with a good understanding of the relationships between the structure and properties of this type of porous polymer.

Currently, in our laboratories, thanks to the results obtained in this work, we are designing and studying the second generation of robust heterogeneous catalytic systems with better transport properties but maintaining the clear advantage of these materials over other polymeric structures due to their higher rigidity in the presence of a large number of solvents, i.e. without undergoing swelling phenomena.

4. Experimental section

4.1. Synthesis of models and porous organic polymers, POPs

4.1.1. Isatin model (IM)

In an oven-dried Schlenk equipped with a magnetic stirrer and blanketed by a nitrogen atmosphere, isatin (3.08 g, 20.6 mmol) and toluene (6.56 mL, 61.8 mmol) were added. The solution was placed into an ice bath, then TFSA (25 mL) was added dropwise for 30 min, and the mixture was stirred at room temperature for 24 h. The dark solution was poured into cold distilled water and the white precipitated was collected and washed with warm distilled water. A white powder was obtained in 71% yield. ^{1}H NMR (500 MHz, $CDCl_3$) δ 7.25–7.20 (m, 2H), 7.18–7.14 (m, 4H), 7.12–7.08 (m, 4H), 7.05 (td, $J = 7.6, 1.0$ Hz, 1H), 6.93 (dt, $J = 7.7, 0.8$ Hz, 1H), 2.31 (s, 6H). ^{13}C NMR (126 MHz, CDCl3) δ 21.01, 62.32, 76.75, 77.00, 77.26, 110.09, 122.76, 126.24, 128.08, 128.26, 129.15, 133.93, 137.00, 138.76, 140.03, 179.91. mp: 204–206 °C. MS (ESI$^+$): m/z 336.1356 $[M^+Na]^+$ (100), 314.1540 $[M^+H]^+$ (17.6), 352.1100, $[M^+K]^+$ (6.7), 627.3015 $[2\ M^+H]^+$ (4.8), 649 $[2\ M^+Na]^+$ (7.3), 962 $[3\ M^+Na]^+$ (1.8), 1275 $[4\ M^+Na]^+$ (9.7), 1589 $[5\ M^+Na]^+$ (7.9). HRMS (ESI$^+$): calculated for $C_{22}H_{19}NNaO$ $[M^+Na]^+$: 336.1359; found: 336.1356. MS (ESI$^+$). Elemental Analysis: calculated ($C_{22}H_{19}NO$) C, 84.31; H, 6.11; N, 4.47; O, 5.10; found C, 84.48; H, 6.24; N, 4.43; O, 5.10.

4.1.2. Methylisatin model (IMMe)

In an oven-dried Schlenk flask equipped with a magnetic stirrer and blanketed by a nitrogen atmosphere, methylisatin (1.00 g, 6.80 mmol) and toluene (2.2 mL, 20.4 mmol) were added. The solution was placed into an ice bath, then TFSA (20 mL) was added dropwise for 30 min, and the mixture was stirred at room temperature. After 24 h, the solution was poured into cold distilled water, neutralized with $NaHCO_3$ and extracted in ethyl acetate. The crude product was purified by chromatographic column, using a mixture of ethyl acetate and hexane in 1: 4 volumetric proportions as eluent. A white powder was obtained with a 59% yield. ^{1}H-RMN (500 MHz, $CDCl_3$) δ: 7.30 (td, $J_{H\text{-}H} = 7.7, 1.2$ Hz, 1H), 6.91 (dt, $J_{H\text{-}H} = 7.8, 0.8$ Hz, 1H), 3.28 (s, 3H), 2.31 (s, 6H), 2.17 (s, 1H). ^{13}C-RMN (101 MHz, $CDCl_3$) δ: 21.15, 26.77, 62.03, 108.55, 122.91, 126.08, 128.41, 129.23, 133.41, 137.35, 139.16, 143.19, 177.97. mp: 120–122 °C.

4.1.3. 135TPB-Isatin POP (IB)

An oven-dried three-neck 500 mL Schlenk flask, equipped with a mechanical stirrer and blanketed by nitrogen 135TPB (5.55 g, 18.1 mmol), isatin (4.00 g, 27.2 mmol), and 10 mL of MSA were mixed. The monomers mixture was stirred for 30 min. The mixture was stirred at room temperature for 15 min and cooled at 0 °C. Then, 40 mL of cold TFSA were added dropwise. After the TFSA addition, the mixture was left to warm up to room temperature and maintained with mechanical stirring for 96 h. The reaction mixture was poured into distilled water, which was neutralized by the addition of a $NaHCO_3$ solution, filtered, and washed sequentially with warm distilled water, methanol, ethyl acetate, and acetone. The product was dried at 180 °C under a 60 mbar dynamic vacuum for 24 h. The material was obtained as a powder in quantitative yield (99.8%). CPMAS SS ^{13}C NMR (11 kHz): δ 179 (broad),142 ppm (broad), 128 ppm (broad), 110 p.m. (broad), 62 ppm (broad). BET Surface Area: 760 m^2/g [49].

4.1.4. Synthesis of POP copolymer 135TPB-isatin-TFAP 4:3:3 (IBT).

An oven-dried three-necked Schlenk flask, 500 mL, equipped with a mechanical stirrer and blanketed by nitrogen, was charged with 135TPB (4.29 g, 14.0 mmol) and isatin (1.50 9 g, 10.4 mmol). The solid monomers were mixed, and MSA (5 mL) was added. The mixture was stirred at room temperature for 15min and cooled at 0 °C. Then, 30 mL of cold TFSA were added dropwise. After the TFSA addition, the mixture was left to warm up to room temperature and maintained with mechanical stirring for 96 h. The reaction mixture was poured into distilled water, neutralized by the addition of a $NaHCO_3$ solution, filtered, and washed sequentially with warm distilled water, methanol, ethyl acetate, and acetone. The product was dried at 180 °C under a 60 mbar dynamic vacuum for 24 h. The material was obtained as a powder in quantitative yield (100%). CPMAS SS ^{13}C NMR (11 kHz): δ 178 (broad),142 ppm (broad), 128 ppm (broad), 109 p.m. (broad), 78 ppm (broad). BET Surface Area: 738 m^2/g [49].

4.1.5. 135TPB-Methylisatin POP (IBMe)

An oven-dried three-neck 500 mL Schlenk flask, equipped with a mechanical stirrer and blanketed by nitrogen 135TPB (4.44 g, 14.5 mmol), methylisatin (3.50 g, 21.7 mmol), and 5 mL of MSA were mixed. The monomers mixture was stirred for 30 min, and the mixture was stirred at room temperature for 15 min and cooled at 0 °C. Then, 35 mL of cold TFSA were added dropwise. After the TFSA addition, the mixture was left to warm up to room temperature and maintained with mechanical stirring for 96 h. The reaction mixture was poured into distilled water, which was neutralized by the addition of a $NaHCO_3$ solution, filtered, and washed sequentially with warm distilled water, methanol, 2-Me THF, ethyl acetate, and acetone. The product was dried at 180 °C under a 60 mbar dynamic vacuum for 24 h. The material was obtained as a powder in quantitative yield (99.6%). CPMAS SS ^{13}C NMR (11 kHz): δ 176 (broad),142 ppm (broad), 127 ppm (broad), 108 p.m. (broad), 61 ppm (broad). BET Surface Area: 835 m^2/g.

4.1.6. Synthesis of 1-Boc-3-((methylsulfonyl)oxy)pyrrolidine (P_0)

In an oven-dried 100 mL Schlenk flask blanketed by nitrogen and magnetically stirred, (R)-1-Boc-3-hydroxypyrrolidine (5.00 g, 26.7 mmol) and Cyrene (30 mL) were added. Then, triethylamine, 5 mL, was added to the Schlenk flask, and the mixture was stirred for 2 h. The mixture was cooled to 0 °C, and methanesulfonyl chloride (2.28 mL, 29.4 mmol) was added. The mixture was allowed to warm up to room temperature and maintained with magnetic stirring for 4 h. The product was poured into distilled water and extracted with ethyl acetate. The organic phase was brought to dryness in a rotary evaporator, and the product **P_0** was obtained as an amber oily solid (88% yield). ^{1}H NMR (500 MHz, $CDCl_3$) δ: 5.24 (m, 1H), 3.75–3.39 (m, 4H), 3.03 (s, 3H), 2.26 (m, 1H), 2.12 (m, 1H), 1.45 (s, 9H).^{13}C NMR (101 MHz, $CDCl_3$) δ 154.14, 79.90, 79.53, 51.91, 43.40, 38.74, 32.23, 28.43. mp: 43–45 °C.

4.1.7. Synthesis 1-Boc 3-(((methylsulfonyl)oxy)methyl) pyrrolidine (P_1)

Into an oven-dried 100 mL Schlenk flask blanketed by nitrogen and magnetically stirred, 1-Boc-3-hydroxymethylpyrrolidine (3.67 mL, 19.9 mmol) and Cyrene (30 mL) were added. Then, triethylamine, 5 mL, was added to the Schlenk flask, and the mixture was stirred for 2 h. The mixture was cooled to 0 °C, and methanesulfonyl chloride (1.70 mL, 21.9 mmol) was slowly added. The mixture was left to warm up to room temperature and maintained with magnetic stirring for 4 h. The product was poured into distilled water and extracted with ethyl acetate. The organic phase was brought to dryness, and the product **P_1** was obtained as an amber foamy solid in a 91% yield. ^{1}H NMR (500 MHz, $CDCl_3$) δ: 4.19 (m, 1H), 4.14 (m, 1H), 3.66–3.40 (m, 2H), 3.35 (m, 1H), 3.21–3.07 (m, 1H), 3.02 (s, 3H), 2.62 (m, 1H), 2.03 (m, 1H), 1.82–1.62 (m, 1H), 1.45 (s, 9H). ^{13}C NMR (101 MHz, $CDCl_3$) δ 154.38, 79.49, 70.25, 48.03, 44.80, 38.38, 37.43, 28.46, 27.59. mp:50–52 °C.

4.1.8. Pyrrolidine functionalized model (IMP_0)

In a 100 mL oven-dried Schlenk flask, under a nitrogen atmosphere, the isatin-toluene model (IM) (0.500 g, 1.60 mmol) was dissolved in 15 mL of Cyrene. Then, Cs_2CO_3 was added (0.520 g, 1.60 mmol) and the mixture was magnetically stirred for 2 h. Subsequently, 1-Boc-3-((methylsulfonyl)oxy)pyrrolidine (**P_0**) (0.445 g, 1.70 mmol) was added; then, the mixture was warmed up to 80 °C, and the reaction was stirred overnight. The product was precipitated in cool distilled water, filtered, washed in distilled water several times. The dried protected model (IMP_0-Boc) was obtained as a white foam. An oven-dried Schlenk flask equipped with magnetic stirring was charged with the protected model (0.700 g, 0.15 mmol) and $CHCl_3$ (3 mL). An excess of TFA (2.0 mL, 2.61 mmol) was added into the flask and the mixture was warmed up at 65 °C and stirred for 24 h. The mixture was left to cool down at RT and neutralized with a $NaHCO_3$ solution. The product dried at 60 °C, 60 mbar, 16 h (IMP_0) was obtained in a 61% yield. ^{1}H NMR (500 MHz, $CDCl_3$) δ 7.25 (m, 3H), 7.10 (m, 9H), 4.85 (m, 1H), 3.36 (m, 2H), 3.13 (m, 1H), 2.9 (m, 1H), 2.31 (s, 6H), 2.13 (m, 2H), 1.99 (s broad, 1H). mp: 96–98 °C. MS (ESI^+): m/z 383.2114 [M+H]+ (100), HRMS (ESI^+): calculated for $C_{26}H_{27}N_2O$ $[M^+H]^+$: 383.2118; found: 383.2114 MS (ESI^+).

4.1.9. Pyrrolidine model (IMP_1)

In a 100 mL oven-dried Schlenk flask, under a nitrogen atmosphere, the isatin-toluene model (IM) (0.500 g, 1.60 mmol) was dissolved in 15 mL of Cyrene. Then, Cs_2CO_3 was added (0.520 g, 1.60 mmol) and the mixture was magnetically stirred for 2 h. Subsequently, 1-Boc-3-(((methylsulfonyl)oxy)methyl) pyrrolidine (**P_1**) (0.468 g, 1.70 mmol) was added; then, the mixture was warmed up to 80 °C and the reaction was stirred overnight. The purified protected model (IMP_1-Boc) was obtained following the same way as that in IMP_0-Boc, as a white foamy solid. An oven-dried Schlenk flask equipped with magnetic stirring was charged with the protected model IMP_1-Boc (0.605 g, 1.20 mmol) and $CHCl_3$ (3 mL). An excess of TFA (2.0 mL, 2.61 mmol) was added to the flask and the mixture was warmed up at 65 °C and stirred for 24 h. The mixture was left to cool down at RT and neutralized with a $NaHCO_3$ solution. The product dried at 60 °C, 60 mbar, 16 h (ITPCH2) was obtained in a 63% yield. ^{1}H NMR (500 MHz, $CDCl_3$) δ 7.27 (m, 2H), 7.10 (m, 9H), 6.96 (d, $J = 7.8$ Hz, 1H), 3.75 (m, 2H), 3.04 (m, 1H), 2.90 (m, 2H), 2.68 (m, 2H), 2.30 (s, 6H), 1.86 (m, 1H), 1.53 (m, 1H). mp: 105–107 °C. **MS** (ESI^+): *m/z* 397.2268 $[M^+H]^+$ (100), 360.3233 (28.4). **HRMS** (ESI^+): calculated for $C_{27}H_{29}N_2O$ $[M^+H]^+$: 397.2274; found: 397.2268 MS (ESI^+).

4.1.10. Functionalization of IB POP (IBP_0-Boc)

An oven-dried Schlenk 100 mL flask, equipped with magnetic stirring and nitrogen blanketed was charged with **IB** (POP 135TPB-isatin) (2.00 g, 6.00 mmol) and Cs_2CO_3 (2.39 g, 7.50 mmol). The mixture of **IB** and Cs_2CO_3 was suspended in 25 mL Cyrene and was let to react for 2 h at RT. Subsequently, **P_0** (1-Boc 3-((methylsulfonyl)oxy)pyrrolidine) (1.67 g, 6.30 mmol) was added and the mixture was warmed up to 80 °C, and maintained with stirring for 48 h. Afterward, the temperature bath was removed and when the mixture reached RT, distilled water was added and the suspension was filtered. The filtered product was washed sequentially with distilled water, and a mixtur of H_2O/MeOH 1:1, MeOH and acetone. The washed product **IBP_0-Boc** was dried at 60 °C, under 60 mbar vacuum for 16 h obtaining a light-yellow powder (99% yield).

4.1.11. IBP_0

On an oven-dried Schlenk flask equipped with magnetic stirring, blanketed by nitrogen, was charged with the functionalized **IBP_0-Boc** (3.00 g, 3.98 mmol) and a mixture of H_2O/MeOH 3:2 was added. An excess of TFA (1.2 mL, 15.92 mmol) was slowly added in the flask. Temperature was raised to the boiling point of TFA and the mixture was stirred for 4 h. Afterward, the mixture was cooled down at RT and neutralized with a $NaHCO_3$ solution. The product was filtered, collected, and purified as the POP functionalized. **IBP_0** was obtained as a light-yellow powder in an 83% yield. CPMAS SS ^{13}C NMR (11 kHz): δ 178 (broad),142 ppm (broad), 128 ppm (broad), 110 pm (broad), 62 ppm (broad), 46 ppm (broad). BET Surface Area: 647 m^2/g. Desorption average pore diameter (4V/A by BET): 2,1214 nm. Pore size: BJH Adsorption average pore diameter (4V/A): 1,3892 nm. BJH Desorption average pore diameter (4V/A): 1,5091 nm.

4.1.12. Functionalization of IB to IBP_1-Boc POPs

An oven-dried Schlenk 100 mL flask, equipped with a magnetic stirrer and nitrogen blanketed, was charged with **IB** (2.00 g, 6.00 mmol) and Cs_2CO_3 (2.39 g, 7.50 mmol). After adding 25 mL of Cyrene, the mixture was put to react for 2 h at RT. Then, P_1(1.76 g, 6.30 mmol) was added and the mixture was warmed up to 80 °C, and stirred for 48 h. Temperature bath was removed and the mixture was cooled at RT, distilled water was added, and the formed solid was collected. The solid was washed sequentially with distilled water, and a mixture of H_2O/MeOH 1:1, MeOH and acetone. The product **IBP_1-Boc** was thoroughly washed and dried at 60 °C, 60 mbar vacuum for 16 h, obtaining a light-yellow powder in a 99% yield.

4.1.13. IBP_1

An oven-dried Schlenk flask equipped with magnetic stirring was charged with **IBP_1-Boc** (3.00 g, 5.81 mmol) and it was suspended in a mixture of H_2O/MeOH 3:2. An excess of TFA (1.8 mL, 23.23 mmol) was added in the flask. Temperature was raised to the boiling point of TFA and the mixture was stirred for 4 h. The mixture was left to cool at RT and neutralized with $NaHCO_3$. The product was washed and dried in the same way as for IBP_0. The product was obtained as a light-yellow powder in a 66% yield. CPMAS SS ^{13}C NMR (11 kHz): δ 177 (broad),143 ppm (broad), 128 ppm (broad), 109 pm (broad), 79 ppm (broad), 45 ppm (broad). BET Surface Area: 511 m^2/g. Adsorption average pore diameter (4V/A by BET): 2.0416 nm. Desorption average pore diameter (4V/A by BET): 1.9457 nm. Pore size: BJH Adsorption average pore diameter (4V/A): 1,7690 nm. BJH Desorption average pore diameter (4V/A): 3.7247 nm.

4.1.14. Synthesis of $IBTP_0$-Boc

An oven-dried Schlenk 100 mL flask equipped with magnetic stirring and nitrogen blanketed was charged with **IBT** (1.50 g, 2.16 mmol) and Cs_2CO_3 (0.86 g, 2.64 mmol). The mixture of **IBT** and Cs_2CO_3 was suspended in 20 mL of Cyrene and was let reacting for 2 h at RT. Subsequently, P_0(1-Boc-3-((methylsulfonyl)oxy) pyrrolidine) (0.60 g, 2.27 mmol) was added and the mixture was warmed up to 80 °C, and maintained with stirring for 48 h. Afterward, the temperature bath was removed and when the mixture reached RT, distilled water was added and the solid suspension was filtered. The filtered product was washed sequentially with distilled water, and a mixture of H_2O/MeOH 1:1, MeOH and acetone. The washed product **$IBTP_0$-Boc** was dried at 60 °C, under 60 mbar vacuum for 16 h, obtaining a light-yellow powder (88% yield).

4.1.15. $IBTP_0$

On an oven-dried Schlenk flask equipped with magnetic stirring, blanketed by nitrogen, was charged with the functionalized POP (**$IBTP_0$-Boc**) (1.15 g, 1.31 mmol) and a mixture of H_2O/MeOH 3:2 was added. Then, an excess of TFA (0.4 mL, 5.23 mmol) was slowly added in the flask and the mixture was warmed at temperature of TFA boiling point and stirred for 4 h. Afterward, the

mixture was cooled down at RT and neutralized with a $NaHCO_3$ solution. The product was filtered, collected, and purified as the POP functionalized. **$IBTP_0$** was obtained as a light-yellow powder in a 99% yield. CPMAS SS ^{13}C NMR (11 kHz): δ 177 (broad),141 ppm (broad), 128 ppm (broad), 109 p.m. (broad), 77 ppm (broad), 64 ppm (broad). BET Surface Area: 794 m^2/g. Pore size: Adsorption average pore diameter (4V/A by BET): 2,2228 nm. BJH Adsorption average pore diameter (4V/A): 1,4781 nm. BJH Desorption average pore diameter (4V/A): 1,5374 nm.

4.1.16. Synthesis of $IBTP_1$-Boc

An oven-dried Schlenk 100 mL flask, equipped with a magnetic stirrer and nitrogen blanked, was charged with **IBT** (2.00 g, 6.00 mmol) and Cs_2CO_3 (2.39 g, 7.50 mmol). After adding 25 mL of Cyrene, the mixture was in reaction for 2 h at RT. Then, 1-Boc-3-methylsulfonyl)oxy)methyl)pyrrolidine, P_1, (1.76 g, 6.30 mmol) was added and the dispersion was warmed up to 80 °C, and stirred for 48 h. Temperature bath was removed and when the mixture was at RT, distilled water was added and the formed solid was collected. The solid was washed sequentially with distilled water, and a mixture of H_2O/MeOH 1:1, MeOH and acetone. The product **$IBTP_1$-Boc** was thoroughly washed with water and dried at 60 °C, 60 mbar vacuum for 16 h, obtaining a light-yellow powder in a 99% yield.

4.1.17. $IBTP_1$

An oven-dried Schlenk flask equipped with magnetic stirring was charged with **$IBTP_1$-Boc** (1.15 g, 1.31 mmol) and a mixture of H_2O/MeOH 3:2 was added. Then, an excess of TFA (0.4 mL, 5.25 mmol) was added in the flask. Temperature was raised to the boiling point of TFA and the mixed solution was stirred for 4 h. The mixture was left to cool at RT and neutralized with $NaHCO_3$. The product was washed and dried as for IBP. The product was obtained as a light-yellow powder in a 97% yield. CPMAS SS ^{13}C NMR (11 kHz): δ 177 (broad),143 ppm (broad), 128 ppm (broad), 109 pm (broad), 79 ppm (broad), 45 ppm (broad). BET Surface Area: 941 m^2/g. **Pore Size** Desorption average pore diameter (4V/A by BET): 3,5619 nm. BJH Adsorption average pore diameter (4V/A): 2,9315 nm. BJH Desorption average pore diameter (4V/A): 29,5670 nm.

4.2. Catalytic study

4.2.1. Formation of nitrones

A solution of $NaHCO_3$ (1 equiv, 0.2 mmol) in EtOH: H_2O (1:1) (0,6 mL) was placed in ultrasonic equipment for 5 min, then, *N*-(*tert*-butyl)hydroxylamine·HCl (1 equiv, 0.2 mmol) was added. The mixture was stirred at room temperature for 5 min. The corresponding polymer weight, and the aldehyde (1 equiv, 0.2 mmol) were added, and the mixture was stirred under the same conditions for the indicated time. The pyrrolidone content of the polymer has been indicated in Tables 2–4, which was calculated according to the catalytic polymer loading (Table 1 and part 5 of the Supporting Information). Afterward, the polymer was filtered, washed with ethyl acetate, and the product was extracted with the same solvent. The organic phase was dried with $MgSO_4$ and evaporated under reduced pressure to obtain the final nitrones without any further purification. The resultant solid was dissolved in $CDCl_3$, and the conversion was determined by NMR. The crude was purified by flash column chromatography using a cyclohexane: acetate 4:1 mixture as eluent.

4.2.2. Polymer recycling procedure

Reaction was started from 50 mg of polymer (equivalent to 0,09 mmol of catalytic pyrrolidine polymer, **IBP_1**). After the reaction proceeded, the mass of employed reagents was recalculated to the amount of recovered polymer after filtration, washing and drying at 50 °C overnight. The washing of the polymer was thoroughly performed by stirring a slurry of polymer and 10 mL MeOH/H_2O (9:1) using an ULTRA-TURRAX device at 6000 rpm for 20 min followed by filtration under vacuum. Table S5 shows the yield and mass of reagents used in each cycle. There is no detrimental effect on the reaction yield, and it is hoped that these results could be extended to reactions operating under flow conditions.

Detailed characterization of nitrone synthesis is described in the supporting information section. Also, all the experimental information related to Knoevenagel reaction, and aldol condensation, catalyzed by the prepared microporous organic polymer networks is included in the Supporting Information.

CRediT author statement

Emily L. Vargas; Validation, Investigation, Writing - Original Draft, Writing - Review and Editing.

Noelia Esteban; Validation, Investigation, Writing - Original Draft.

Javier Cencerrero; Validation, Investigation.

Victoria Francés; Validation, Investigation.

Cristina Álvarez; Validation, Methodology, Formal analysis.

Jesús A. Miguel, Conceptualization, Methodology, Formal analysis, Supervision, Resources.

Alberto Gallardo; Validation, Methodology, Formal analysis, Writing - Review and Editing.

Angel E. Lozano; Conceptualization, Methodology, Resources, Writing - Original Draft, Writing - Review and Editing, Funding acquisition.

M. Belén Cid; Conceptualization, Methodology, Resources, Supervision, Writing - Original Draft, Writing - Review and Editing, Funding acquisition.

Declaration of competing interest

The authors declare that they have no known competing financial interests or personal relationships that could have appeared to influence the work reported in this paper.

Acknowledgements

We acknowledge the Spanish Government (Agencia Estatal de Investigación projects; CTQ2016-78779-R, PID2019-109403RB-C22, RTI2018-096328-B-I00, CTQ2017-89217-P and PID2020-118547GB-I00), and the Regional Government of Castilla y León (project CyL and EU-FEDER program VA224P20), for financial support. E. L. Vargas thanks University of Costa Rica for a PhD scholarship. We must thank Rebecca Chevillard and Valentina Petrelli for some preliminary experiments.

Appendix A. Supplementary data

Supplementary data to this article can be found online at https://doi.org/10.1016/j.mtchem.2022.100966.

References

[1] B. Gates, Catalityc chemistry, Catalityc Chem. (1992) 458.
[2] G.A. Somorjai, On the move, Nature 430 (2004), https://doi.org/10.1038/430730a, 730–730.
[3] K.T. Wan, M.E. Davis, Design and synthesis of a heterogeneous asymmetric catalyst, Nature 370 (1994) 449–450, https://doi.org/10.1038/370449a0.
[4] D.S. Su, S. Perathoner, G. Centi, Nanocarbons for the development of advanced catalysts, Chem. Rev. 113 (2013) 5782–5816, https://doi.org/10.1021/cr300367d.

[5] C.J. Li, B.M. Trost, Green chemistry for chemical synthesis, Proc. Natl. Acad. Sci. U.S.A. 105 (2008) 13197–13202, https://doi.org/10.1073/pnas.0804348105.
[6] V.K. Dioumaev, R.M. Bullock, A recyclable catalyst that precipitates at the end of the reaction, Nature 424 (2003) 530–532, https://doi.org/10.1038/nature01856.
[7] J.M.J. Frechet, M.V. De Meftahi, Poly (Viny1 pyridine) s : simple reactive polymers with multiple applications, Br. Polym. J. 16 (1984) 193–198.
[8] P. Li, J. Du, Y. Xie, M. Tao, W.Q. Zhang, Highly efficient polyacrylonitrile fiber catalysts functionalized by aminopyridines for the synthesis of 3-substituted 2-aminothiophenes in water, ACS Sustain. Chem. Eng. 4 (2016) 1139–1147, https://doi.org/10.1021/acssuschemeng.5b01216.
[9] Y. He, C. Cai, Polymer-supported macrocyclic Schiff base palladium complex: an efficient and reusable catalyst for Suzuki cross-coupling reaction under ambient condition, Catal. Commun. 12 (2011) 678–683, https://doi.org/10.1016/j.catcom.2010.12.017.
[10] M.J. Climent, A. Corma, S. Iborra, M.J. Sabater, Heterogeneous catalysis for tandem reactions, ACS Catal. 4 (2014) 870–891, https://doi.org/10.1021/cs401052k.
[11] C. Sievers, S.L. Scott, Y. Noda, L. Qi, E.M. Albuquerque, R.M. Rioux, Phenomena affecting catalytic reactions at solid–Liquid interfaces, ACS Catal. 6 (2016), https://doi.org/10.1021/acscatal.6b02532.
[12] N. Kosinov, C. Liu, E.J.M.M. Hensen, E.A. Pidko, Engineering of transition metal catalysts confined in zeolites, Chem. Mater. 30 (2018) 3177–3198, https://doi.org/10.1021/acs.chemmater.8b01311.
[13] T.A. Shifa, A. Vomiero, Confined catalysis: progress and prospects in energy conversion, Adv. Energy Mater. 9 (2019) 1–15, https://doi.org/10.1002/aenm.201902307.
[14] R. Gramage-Doria, J.N.H. Reek, Organocatalysis in confined spaces, ChemCatChem 5 (2013) 677–679, https://doi.org/10.1002/cctc.201200801.
[15] Q. Fu, X. Bao, Confined microenvironment for catalysis control, Nat. Catal. 2 (2019) 834–836, https://doi.org/10.1038/s41929-019-0354-z.
[16] V. Mouarrawis, R. Plessius, J.I. van der Vlugt, J.N.H. Reek, Confinement effects in catalysis using well-defined materials and cages, Front. Chem. 6 (2018) 623, https://doi.org/10.3389/fchem.2018.00623.
[17] X.S. Zhao, X.Y. Bao, W. Guo, F.Y. Lee, Immobilizing catalysts on porous materials, Mater. Today 9 (3) (2006) 32–39, https://doi.org/10.1016/S1369-7021(06)71388-8.
[18] F. Goettmann, C. Sanchez, How does confinement affect the catalytic activity of mesoporous materials? J. Mater. Chem. 17 (2007) 24–30, https://doi.org/10.1039/B608748P.
[19] C. Guo, J. Xiao, Towards unifying the concepts of catalysis in confined space, Comput. Mater. Sci. 161 (2019) 58–63, https://doi.org/10.1016/j.commatsci.2019.01.039.
[20] W.Y. Gao, A.D. Cardenal, C.H. Wang, D.C. Powers, In operando analysis of diffusion in porous metal-organic framework catalysts, Chem. Eur J. 25 (2019) 3465–3476, https://doi.org/10.1002/chem.201804490.
[21] F. Yang, D. Deng, X. Pan, Q. Fu, X. Bao, Understanding nano effects in catalysis, Natl. Sci. Rev. 2 (2015) 183–201, https://doi.org/10.1093/nsr/nwv024.
[22] A. Erkkilä, I. Majander, P.M. Pihko, Iminium catalysis, Chem. Rev. 107 (2007) 5416–5470, https://doi.org/10.1021/cr068388p.
[23] J.L. Vicario, E. Reyes, D. Badía, L. Carrillo, Catalytic Asymmetric Conjugate Reactions, Wiley VCH, Weinheim, 2010, https://doi.org/10.1002/9783527630578.ch6.
[24] P.I. Dalko, Comprehensive Enantioselective Organocatalysis, Wiley-VCH Verlag GmbH & Co. KGaA, Weinheim, Germany, 2013, https://doi.org/10.1002/9783527658862.
[25] M. Nielsen, D. Worgull, T. Zweifel, B. Gschwend, S. Bertelsen, K.A. Jørgensen, Mechanisms in aminocatalysis, Chem. Commun. 47 (2011) 632–649, https://doi.org/10.1039/C0CC02417A.
[26] A. Vega-Peñaloza, S. Paria, M. Bonchio, L. Dell'Amico, X. Companyó, Profiling the privileges of pyrrolidine-based catalysts in asymmetric synthesis: from polar to light-driven radical chemistry, ACS Catal. 9 (2019) 6058–6072, https://doi.org/10.1021/acscatal.9b01556.
[27] M.E. Belowich, J.F. Stoddart, Dynamic imine chemistry, Chem. Soc. Rev. 41 (2012) 2003, https://doi.org/10.1039/c2cs15305j.
[28] S. Morales, F.G. Guijarro, J.L. García Ruano, M.B. Cid, A general aminocatalytic method for the synthesis of aldimines, J. Am. Chem. Soc. 136 (2014) 1082–1089, https://doi.org/10.1021/ja4111418.
[29] S. Morales, F.G. Guijarro, I. Alonso, J.L. García Ruano, M.B. Cid, Dual role of pyrrolidine and cooperative pyrrolidine/pyrrolidinium effect in nitrone formation, ACS Catal. 6 (2016) 84–91, https://doi.org/10.1021/acscatal.5b01726.
[30] S. Morales, J.L. Aceña, J.L. García Ruano, M.B. Cid, Sustainable synthesis of oximes, hydrazones, and thiosemicarbazones under mild organocatalyzed reaction conditions, J. Org. Chem. 81 (2016) 10016–10022, https://doi.org/10.1021/acs.joc.6b01912.
[31] E.L. Vargas, J.A. Velázquez, E. Rodrigo, H. Reinecke, J. Rodríguez-Hernández, A. Fernández-Mayoralas, A. Gallardo, M.B. Cid, p K a modulation of pyrrolidine-based catalytic polymers used for the preparation of glycosyl hydrazides at physiological pH and temperature, ACS Appl. Bio Mater. 3 (2020) 1955–1967, https://doi.org/10.1021/acsabm.9b01123.
[32] Z.-J. Lin, J. Lü, L. Li, H.-F. Li, R. Cao, Defect porous organic frameworks (dPOFs) as a platform for chiral organocatalysis, J. Catal. 355 (2017) 131–138, https://doi.org/10.1016/j.jcat.2017.09.014.
[33] P. Bhanja, S. Chatterjee, A. Bhaumik, Triazine-based porous organic polymer with good CO 2 gas adsorption properties and an efficient organocatalyst for the one-pot multicomponent condensation reaction, ChemCatChem 8 (2016) 3089–3098, https://doi.org/10.1002/cctc.201600840.
[34] Q. Sun, Z. Dai, X. Meng, F.-S. Xiao, Porous polymer catalysts with hierarchical structures, Chem. Soc. Rev. 44 (2015) 6018–6034, https://doi.org/10.1039/C5CS00198F.
[35] V. Pascanu, G. González Miera, A.K. Inge, B. Martín-Matute, Metal–organic frameworks as catalysts for organic synthesis: a critical perspective, J. Am. Chem. Soc. 141 (2019) 7223–7234, https://doi.org/10.1021/jacs.9b00733.
[36] X. Cao, Z. Wang, Z. Qiao, S. Zhao, J. Wang, Penetrated COF channels: amino environment and suitable size for CO 2 preferential adsorption and transport in mixed matrix membranes, ACS Appl. Mater. Interfaces 11 (2019) 5306–5315, https://doi.org/10.1021/acsami.8b16877.
[37] J. Bi, Y. Dong, D. Meng, D. Zhu, T. Li, The study and application of three highly porous hyper-crosslinked catalysts possessing similar catalytic centers, Polymer 164 (2019) 183–190, https://doi.org/10.1016/j.polymer.2019.01.009.
[38] M.S. Lohse, T. Bein, Covalent organic frameworks: structures, synthesis, and applications, Adv. Funct. Mater. 28 (2018) 1705553, https://doi.org/10.1002/adfm.201705553.
[39] H. Xu, X. Chen, J. Gao, J. Lin, M. Addicoat, S. Irle, D. Jiang, Catalytic covalent organic frameworks via pore surface engineering, Chem. Commun. 50 (2014) 1292–1294, https://doi.org/10.1039/C3CC48813F.
[40] H. Xu, J. Gao, D. Jiang, Stable, crystalline, porous, covalent organic frameworks as a platform for chiral organocatalysts, Nat. Chem. 7 (2015) 905–912, https://doi.org/10.1038/nchem.2352.
[41] K. Cho, J. Yoo, H.-W. Noh, S.M. Lee, H.J. Kim, Y.-J. Ko, H.-Y. Jang, S.U. Son, Hollow structural effect of microporous organocatalytic polymers with pyrrolidines: dramatic enhancement of catalytic performance, J. Mater. Chem. A. 5 (2017) 8922–8926, https://doi.org/10.1039/C7TA02404E.
[42] S.I. Murahashi, Y. Imada, Synthesis and transformations of nitrones for organic synthesis, Chem. Rev. 119 (2019) 4684–4716, https://doi.org/10.1021/acs.chemrev.8b00476.
[43] J.M. Carney, R.A. Floyd, Protection against oxidative damage to CNS by α-phenyl-tert-butyl nitrone (PBN) and other spin-trapping agents: a novel series of nonlipid free radical scavengers, J. Mol. Neurosci. 3 (1991) 47–57, https://doi.org/10.1007/BF02896848.
[44] C.E. Thomas, D.F. Ohlweiler, A.A. Carr, T.R. Nieduzak, D.A. Hay, G. Adams, R. Vaz, R.C. Bernotas, Characterization of the radical trapping activity of a novel series of cyclic nitrone spin traps, J. Biol. Chem. 271 (1996) 3097–3104, https://doi.org/10.1074/jbc.271.6.3097.
[45] R.A. Floyd, R.D. Kopke, C.-H. Choi, S.B. Foster, S. Doblas, R.A. Towner, Nitrones as therapeutics, Free Radic. Biol. Med. 45 (2008) 1361–1374, https://doi.org/10.1016/j.freeradbiomed.2008.08.017.
[46] A.L. Lira, M.G. Zolotukhin, L. Fomina, S. Fomine, Triflic-acid-mediated polycondensation of carbonyl compounds with aromatic hydrocarbons - a theoretical study, Macromol. Theory Simulations 16 (2007) 227–239, https://doi.org/10.1002/mats.200600084.
[47] M.T. Guzmán-Gutiérrez, D.R. Nieto, S. Fomine, S.L. Morales, M.G. Zolotukhin, M.C.G. Hernandez, H. Kricheldorf, E.S. Wilks, M.T. Guzmán-Gutiérrez, D.R. Nieto, S. Fomine, S.L. Morales, M.G. Zolotukhin, M.C.G. Hernandez, H. Kricheldorf, E.S. Wilks, Dramatic enhancement of superacid-catalyzed polyhydroxyalkylation reactions, Macromolecules 44 (2011) 194–202, https://doi.org/10.1021/ma102267f.
[48] L.I. Olvera, F.A. Ruiz-Treviño, J. Balmaseda, I.A. Ronova, M.G. Zolotukhin, M.P. Carreón-Castro, E. Lima, J. Cárdenas, R. Gaviño, Microporous polymers from superacid catalyzed polymerizations of fluoroketones with p-quaterphenyl: synthesis, characterization, and gas sorption properties, Polymer 102 (2016) 221–230, https://doi.org/10.1016/j.polymer.2016.09.021.
[49] B. Lopez-Iglesias, F. Suárez-García, C. Aguilar-Lugo, A. González Ortega, C. Bartolomé, J.M. Martínez-Ilarduya, J.G. de la Campa, Á.E. Lozano, C. Álvarez, Microporous polymer networks for carbon capture applications, ACS Appl. Mater. Interfaces 10 (2018) 26195–26205, https://doi.org/10.1021/acsami.8b05854.
[50] Z.J. Wang, S. Ghasimi, K. Landfester, K.A.I. Zhang, Highly porous conjugated polymers for selective oxidation of organic sulfides under visible light, Chem. Commun. 50 (2014) 8177–8180, https://doi.org/10.1039/c4cc02861a.
[51] K.D. Ahn, Y.H. Lee, D.I. Koo, Synthesis and polymerization of N-(tert-butyloxycarbonyl)maleimide and facile deprotection of polymer side-chain t-BOC groups, Polymer 33 (1992) 4851–4856, https://doi.org/10.1016/0032-3861(92)90702-X.
[52] W.C. Griffin, Calculation of HLB values of non-ionic surfactants, J. Soc. Cosmet. Chem. 5 (1954) 249–256.
[53] J.N. Appaturi, R. Ratti, B.L. Phoon, S.M. Batagarawa, I.U. Din, M. Selvaraj, R.J. Ramalingam, A review of the recent progress on heterogeneous catalysts for Knoevenagel condensation, Dalt. Trans. 50 (2021) 4445–4469, https://doi.org/10.1039/d1dt00456e.